

**SPECTRAL AND MINERALOGICAL ANALYSIS OF CHANG'E-5 CANDIDATE LANDING SITE IN NORTHERN OCEANUS PROCELLARUM** Zongcheng Ling<sup>1</sup>, Changqing Liu<sup>1</sup>, B. L. Jolliff<sup>2</sup>, Jiang Zhang<sup>1</sup>, Bo, Li<sup>1</sup>, Lingzhi Sun<sup>1</sup>, Jian Chen<sup>1</sup>, Jianzhong Liu<sup>3</sup> <sup>1</sup>Shandong Provincial Key Laboratory of Optical Astronomy and Solar-Terrestrial Environment, Institute of Space Sciences, Shandong University, Weihai, 264209, China; <sup>2</sup>Dept Earth & Planetary Sciences and McDonnell Center for the Space Sciences, Washington University in St. Louis; <sup>3</sup>Institute of Geochemistry, Chinese Academy of Sciences, Guiyang 550002, China ([zcling@sdu.edu.cn](mailto:zcling@sdu.edu.cn)).

**Introduction:** A new lunar sample-return mission, China's Chang'e-5, has been planned to return the first new samples from the Moon in 40 years since Luna 24. One candidate landing site is the northern Oceanus Procellarum [1, 2]. The different basaltic units have complex extrusive and flooding history. Mare basalts contain information about the lunar mantle, and reflects the diversity of their source regions. Chang'e-3's Yutu rover has provided some ground truth of young mare basaltic rocks in Mare Imbrium [3, 4], moreover we hope Chang'e-5 would lead to new information about the lunar interior and thermal evolution history, which can be studied in detail by returned samples in the laboratory. Here we conduct a spectral survey of small craters in this region, with the intent to give a compositional constraint on different mare units. The spectral data, mineral modes, and mineral chemistries of the Chang'e-5 landing site from a remote sensing view would help to evaluate the science potential of the returned samples, which should be better understood before the mission's operations in late 2017.

We employ orbital hyperspectral imaging data from Chandrayaan-1 Moon Mineralogy Mapper (M<sup>3</sup>) to evaluate the spectral and compositional variations of the three basaltic units (P9, P10, and P58 from Hiesinger et al. [5], shown in Fig. 1a), near Mons Rümker. These three units show distinct colors in the false color image (Fig. 1b). The lower and upper red unit (P9 and P10) are much older (~3.5 Ga) than the bluish unit P58 (1.33 Ga).

**Spectral and mineral characteristics of three units:** The spectra of small craters in basaltic units are good candidates for spectral survey due to their sharp spectral features devoid of space weathering effects. We have carefully chosen hundreds of craters with sharp visible and near-infrared spectra features for detailed study of the mineralogy and geochemistry in this area. The crater diameters are constrained by less than ~500 m to reduce the possible mixing effects from underlying basaltic units. Fig. 1a shows the locations of three small craters for which we selected representative spectra of the three basaltic units (P9, P10, and P58). The spectra of three fresh craters (Fig. 1a) in each unit with the most obvious spectral features are chosen as representative spectra. As shown by three representative spectra in Fig. 2, all three basaltic units are dominated by pyroxene and olivine.

However, the spectra taken from the younger P58 unit (1.33 Ga) show distinct features from the other two, i.e., more broad 1- $\mu$ m features indicating abundant olivine.

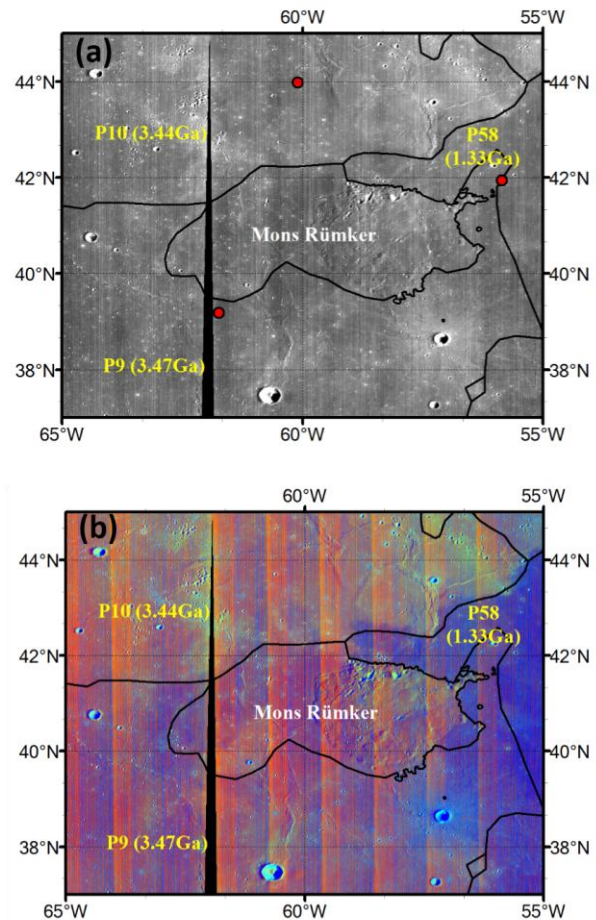


**Figure 1.** Three basaltic units (P9, P10, and P58 from Hiesinger et al. 2003 [5]) in northern Oceanus Procellarum near Mons Rümker. (a) Chandrayaan-1 M<sup>3</sup> mosaic, red spots indicate three small craters whose spectra are extracted to represent the fresh spectra of three units. (b) False color image, R = spectral slope, G = 1658 nm reflectance, B = absorption depth of the 1- $\mu$ m absorption feature.

Modified Gaussian Modeling (MGM) deconvolution is conducted for the M<sup>3</sup> spectral data similar to the method in [7]. The derived peak positions of High-Ca (HCP), Low-Ca (LCP) pyroxenes and Olivine of each

unit are shown in Table 1. All three units have more abundant HCP than LCP ( $HCP/LCP \approx 1.6$ ), while the P58 unit has much more abundant olivine than the other two units ( $HCP/OL \approx 1.0$  for P58). The derived olivine peak positions (0.87  $\mu m$ , 1.08  $\mu m$ , 1.24  $\mu m$ ) indicate their relatively Fe-rich nature ( $Fo \sim 50$ ). We can also easily find that the pyroxene and olivine chemistries P58 are similar to those measured by the Yutu rover (see [7]), but with even higher proportions ( $HCP/OL \approx 1.0$  for P58 versus  $HCP/OL \approx 2.0$  for CE3-0005) of olivine in the basaltic rocks.

**Conclusions:**

Young volcanism of the Moon is important for us to understand mantle evolution of the Moon. Our study provides some mineralogical information about different units around Mons Rümker. We anticipate that future lunar sample return will test our predictions and provide new ground truth from our nearest neighbor satellite. Moreover, landing on the young age unit P58 will probably return the youngest lunar basaltic samples with less safety hazards (i.e. may meet less craters in the younger smooth lava plain). Those basaltic samples, probably similar to Chang'e-3

landing are very precious for our understanding of late-stage volcanism on the Moon.

The candidate landing region of Chang'e-5 mission in this study including the three basaltic units would be a good landing area for evaluating the compositional properties of the young and old basaltic units, and the chronology data is especially critical for the evaluation of the lunar impact-crater statistics and planetary remotely sensed chronology [5]. Sampling the lunar soils and rocks in this area will help to decipher some of the mysteries in late-stage volcanism on the Moon.

**Acknowledgements:** This research was supported partially by the National Natural Science Foundation of China (41473065, 41373068), Natural Science Foundation of Shandong Province (JQ201511 and ZR2015DQ001), Qilu (Tang) Young Scholars Program of Shandong University, Weihai (2015WHWLJH14) for ZCL, and partially by Washington University in St. Louis for BLJ and ZCL.

**References:** [1] Li et al., (2012), AGU, #P43B-1927. [2] Zhao et al., (2016) LPSC, 1758. [3] Xiao et al. (2015) Science 347, 1226–1229. [4] Ling, et al. (2015) *Nat. Comm.* 6:8880, doi: 10.1038/ncomms9880 [5] Hiesinger et al. (2003), *J. Geophys. Res.*, 108(E7), 5065.

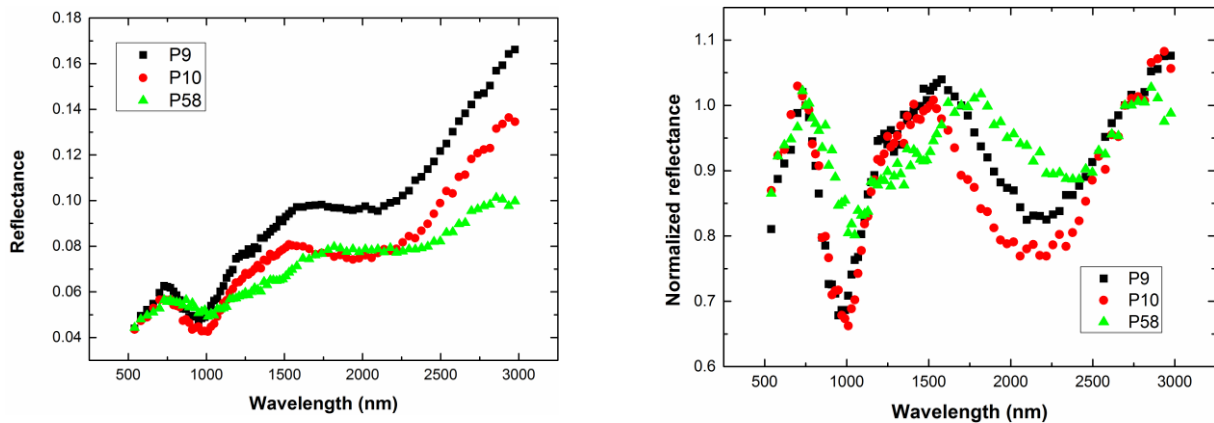


**Figure 2.** The three representative visible near-infrared spectra of P9, P10 and P58 units from M<sup>3</sup> data

**Table 1.** MGM results of the three representative VNIS spectra.

| Spectrum                          | P9                                 |      |          | P10                                |      |          | P58                                |      |          |
|-----------------------------------|------------------------------------|------|----------|------------------------------------|------|----------|------------------------------------|------|----------|
|                                   | Center                             | FWHM | Strength | Center                             | FWHM | Strength | Center                             | FWHM | Strength |
| Olivine                           | 866                                | 113  | -0.068   | 863                                | 95   | -0.107   | 869                                | 117  | -0.020   |
|                                   | 1084                               | 125  | -0.109   | 1079                               | 133  | -0.179   | 1065                               | 96   | -0.137   |
|                                   | 1237                               | 256  | -0.068   | 1228                               | 292  | -0.059   | 1247                               | 338  | -0.122   |
| HCP                               | 987                                | 167  | -0.229   | 990                                | 131  | -0.244   | 987                                | 85   | -0.121   |
|                                   | 2256                               | 429  | -0.192   | 2277                               | 425  | -0.229   | 2401                               | 301  | -0.105   |
| LCP                               | 927                                | 150  | -0.147   | 927                                | 131  | -0.156   | 922                                | 88   | -0.061   |
|                                   | 1909                               | 393  | -0.093   | 1907                               | 395  | -0.181   | 2100                               | 300  | -0.058   |
| HCP/LCP (1 $\mu m$ ratio)         | 1.6 (LCP/(LCP+HCP) $\approx$ 0.39) |      |          | 1.6 (LCP/(LCP+HCP) $\approx$ 0.39) |      |          | 2.0 (LCP/(LCP+HCP) $\approx$ 0.34) |      |          |
| HCP/LCP (2 $\mu m$ ratio)         | 2.1 (LCP/(LCP+HCP) $\approx$ 0.33) |      |          | 1.3 (LCP/(LCP+HCP) $\approx$ 0.44) |      |          | 1.8 (LCP/(LCP+HCP) $\approx$ 0.36) |      |          |
| HCP/OL (1 $\mu m$ /1.25 $\mu m$ ) | 3.3 (OL/(OL+HCP) $\approx$ 0.23)   |      |          | 4.2 (OL/(OL+HCP) $\approx$ 0.19)   |      |          | 1.0 (OL/(OL+HCP) $\approx$ 0.50)   |      |          |